Caloric response of Fe$_{49}$Rh$_{51}$ subjected to uniaxial load and magnetic field

Adrià Gràcia-Condal,[1] Enric Stern-Taulats,[1,2] Antoni Planes,[1] and Lluís Mañosa[1]

[1]*Departament de Física de la Matèria Condensada, Facultat de Física, Universitat de Barcelona,*
Martí i Franquès 1, E-08028 Barcelona, Catalonia
[2]*Department of Materials Science, University of Cambridge, 27 Charles Babbage Road, Cambridge CB3 0FS, United Kingdom*

We have used differential scanning calorimetry and thermometry techniques under applied magnetic field and compressive uniaxial stress to determine isothermal entropy and adiabatic temperature changes that quantify the caloric effects associated with the magnetostructural transition of an Fe$_{49}$Rh$_{51}$ alloy. It is found that the transition temperature increases with increasing compressive stress while it decreases for increasing tensile stress. This behavior gives rise to a conventional elastocaloric effect for compressive stresses in contrast to the reported inverse elastocaloric effect for tensile stresses. The combined effect of stress and magnetic field does not lead to a significant increase of the maximum temperature and entropy changes associated with magnetocaloric and elastocaloric effects, but there is a modification of the temperature window where the sample exhibits giant caloric responses.

I. INTRODUCTION

Giant caloric materials display large entropy and temperature changes upon the isothermal and adiabatic application (or removal) of external fields, respectively [1–3]. For most of these materials, the giant caloric effect is associated with a field-induced ferroic phase transition, where the latent heat of the transition provides the major contribution to the caloric entropy change. Caloric effects are classed by the nature of the applied external field such as magnetocaloric [4], electrocaloric [5], and mechanocaloric [6] for magnetic, electric and mechanical fields, respectively. While magnetic and electric fields are vectors (rank-one tensors), stress is a rank-two tensor and even for isotropic materials two experiments under two independent stress-tensor components are required for a complete description of mechanocaloric effects. The response to uniaxial stress is known as elastocaloric effect [7], and the response to hydrostatic pressure as barocaloric effect [8].

Many caloric materials are multiferroics and exhibit a ferroic phase transition which is sensitive to more than one external field. Such an interplay between different degrees of freedom enables to tune the properties of a given caloric effect by means of a secondary field (not conjugated to the main ferroic property) [9], and in some cases the cooperative application of two external fields can give rise to multicaloric effects [10–12]. The research in multicaloric materials is gaining interest [12] since, on the one hand, they provide an excellent framework to study the physics of phase transitions with coupled degrees of freedom, and on the other hand, there are good prospects that application of multiple external fields can help in overcoming a number of the limitations (such as hysteresis and reduced temperature window) in future application of caloric and multicaloric materials in clean and efficient solid-state refrigeration [13].

Interestingly enough, giant magnetocaloric [14] and elastocaloric [15] properties were reported in Fe-Rh well before the publication of the seminal reports of giant magnetocaloric effects on Gd-Si-Ge [16] and elastocaloric effects on Cu-Zn-Al [7] that fuelled the research in these topics. In spite of these early reports, studies of Fe-Rh were very scarce, mainly because it was believed that their caloric properties were not reproducible. However, recently, Fe-Rh has received considerable attention [17], and a good reproducibility upon magnetic field cycling has been demonstrated [18–20] for properly prepared samples. Furthermore, giant and reproducible barocaloric effects have also been found in this material [18], and the multicaloric response under the combined action of magnetic field and hydrostatic pressure has very recently been characterized [11]. It turns out that Fe-Rh is nowadays considered one of the benchmark caloric and multicaloric materials [21].

In Fe-Rh, giant caloric effects originate from a first-order metamagnetic phase transition from a high-temperature ferromagnetic (FM) phase to a low-temperature antiferromagnetic (AFM) phase [22]. There is no change in crystal symmetry at the phase transition (both phases have a CsCl crystal structure) with a volume of the FM phase ∼1% larger than that of the AFM phase. The changes in magnetization and volume make the phase transition sensitive to the application of magnetic and mechanical fields. The giant caloric response of Fe-Rh when subjected to magnetic or mechanical fields (or a combination of both) is associated with the latent heat of the first-order magnetostructural transition (and thereby to the transition entropy change), which provides the major contribution to the field-induced isothermal entropy change. At the phase transition, there are changes in electron and phonon densities of states. The former provides the electronic and magnetic contributions and the latter provides the lattice contribution to the total entropy change. Recently, density functional theory has been used to compute the thermodynamic quantities associated with caloric effects in Fe-Rh [23]. These calculations suggest that the lattice contribution to the caloric

effect is small compared to the sum of electronic and magnetic contributions. The computed isothermal entropy changes and adiabatic temperature changes are in quantitative agreement with experimental data.

In spite of the early report of elastocaloric adiabatic temperature changes in Fe-Rh wires subjected to tensile stresses [15], no further studies were performed along this line, and a complete characterization of the elastocaloric properties of this compound is still lacking. In particular, no data for isothermal entropy changes are available. One of the objectives of the present work is to provide a thorough characterization of the elastocaloric properties of Fe-Rh when subjected to uniaxial compressive stresses. Different elastocaloric behavior has been found depending on whether uniaxial stresses are compressive or tensile. A second objective of the work is to determine the caloric properties of Fe-Rh when subjected to the combined action of magnetic field and uniaxial stress. Present results, together with our previous study [11] of the behavior under hydrostatic pressure and magnetic field provide a complete characterization of the multicaloric response of this relevant compound under magnetic and mechanical fields.

II. EXPERIMENTAL DETAILS

A polycrystalline sample of nominal composition $Fe_{49}Rh_{51}$ was prepared by arc melting. The specimen used for both calorimetric and thermometric experiments was a 3.3 mm $\times$ 3.0 mm $\times$ 5.6 mm parallelepiped sample. Details on sample preparation and heat treatment are given in Refs. [11,18,19].

Calorimetric measurements were conducted by means of a bespoke calorimeter, which operates in a temperature range 200–400 K, under magnetic fields in the range 0–6 T and compressive uniaxial loads up to 1.2 kN. The calorimeter operates under two different modes: (i) scanning magnetic field at constant temperature and (ii) scanning temperature at constant magnetic field. In both cases a selected applied load is kept constant. The device is described in detail in Ref. [24]

Temperature changes resulting from the application and removal of magnetic fields under applied uniaxial compressive load were measured by means of a purpose built experimental system (see Fig. 1). The $Fe_{49}Rh_{51}$ sample (a) is placed between the poles of an electromagnet, and lies on top of a 3.5 mm thickness polyether ether ketone (PEEK) disk, (b) which sits on top of a high-strength aluminium container (c). Uniaxial load is applied by means of a screw (d) that pushes a free mobile high-strength aluminium rod (e). To minimize thermal losses between the specimen and the rod, a second 2.5 mm thickness PEEK disk (b) is placed between the upper face of the sample and the bottom part of the mobile rod. The applied load is measured by a load cell (f) placed between the upper part of the mobile rod and the lower part of the screw. The specimen temperature is measured by a fine gauge K thermocouple (0.075 mm diameter) (g), which is attached to a free surface of the specimen. Temperature control is achieved by circulating a cryofluid through the bottom container, and the temperature of this fluid is controlled by a Lauda Proline thermal bath. The applied magnetic field is measured by a Hall probe (h) placed next to the sample. The region surrounding the sample is covered with polystyrene to improve adiabaticity of the experiments. The maximum applied load is 1 kN. The
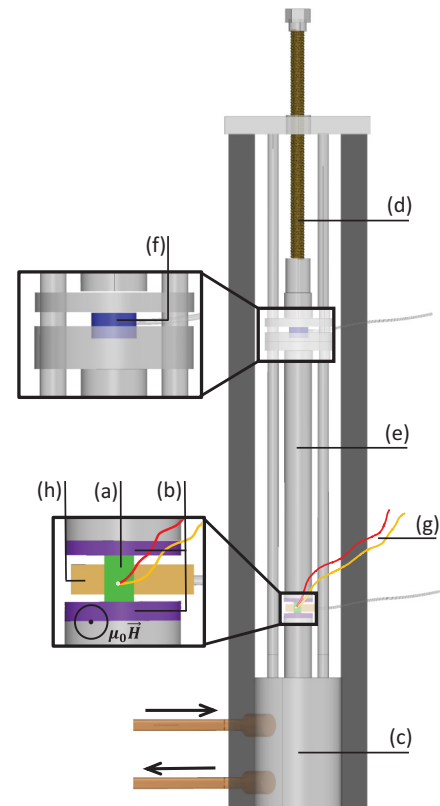

FIG. 1. Sketch of the experimental setup to measure temperature changes under uniaxial load and magnetic field. (a) sample, (b) PEEK disk, (c) container, (d) screw, (e) aluminium rod, (f) load cell, (g) thermocouple, and (h) Hall probe.

operating temperature range is 270–350 K, and the magnetic field range is 0–1.7 T. Application (removal) of magnetic field at the highest possible rate (1.5 T s^{-1}) occurs at much lower time intervals than the time constant associated with the heat exchange between the sample and the surroundings, and the experiments can be considered close to adiabatic conditions.

III. EXPERIMENTAL RESULTS

A. Calorimetric measurements

Examples of thermal curves recorded during heating and cooling runs at selected values of applied (constant) magnetic field and uniaxial compressive stress [25] are shown in Fig. 2. On heating [Fig. 2(a)], the endothermal peak is associated with the AFM to FM transition while the exothermal peak on cooling [Fig. 2(b)] corresponds to the FM to AFM transition. Because of the complexity linked to the application of stress, our calorimeter does not enable a control of temperature ramps as good as the one in conventional DSC, and isofield calorimetric curves exhibit a poor baseline. On the other hand, in the isothermal mode (scanning magnetic field), there is a much better baseline, as illustrated in Figs. 2(c) and 2(d), which show examples of thermal curves recorded upon increasing and decreasing the magnetic field at selected (constant) values of temperature and uniaxial compressive stress. Positive (endothermal) signals correspond to the AFM-FM transition taking place upon increasing magnetic field while negative
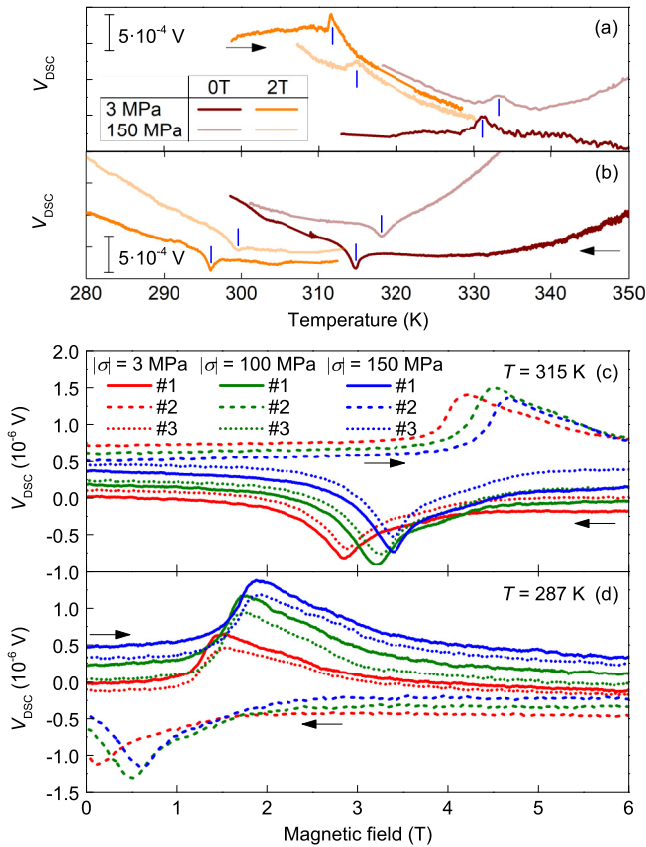
FIG. 2. Thermal curves recorded during heating (a) and cooling (b) runs at selected constant values of magnetic field and uniaxial compressive stresses. The transition temperatures (corresponding to the calorimetric peaks) for the AFM to FM (a) and FM to AFM (b) transitions are indicated by short vertical blue lines. (c) and (d) show illustrative examples of isothermal calorimetric curves recorded while sweeping magnetic field at selected values of temperature and uniaxial compressive stresses. Positive curves correspond to the endothermal AFM to FM transition and negative curves, to the exothermal FM to AFM transition. Solid lines correspond to the first application (and first removal) of magnetic field and dashed and dotted lines to subsequent field cycling.
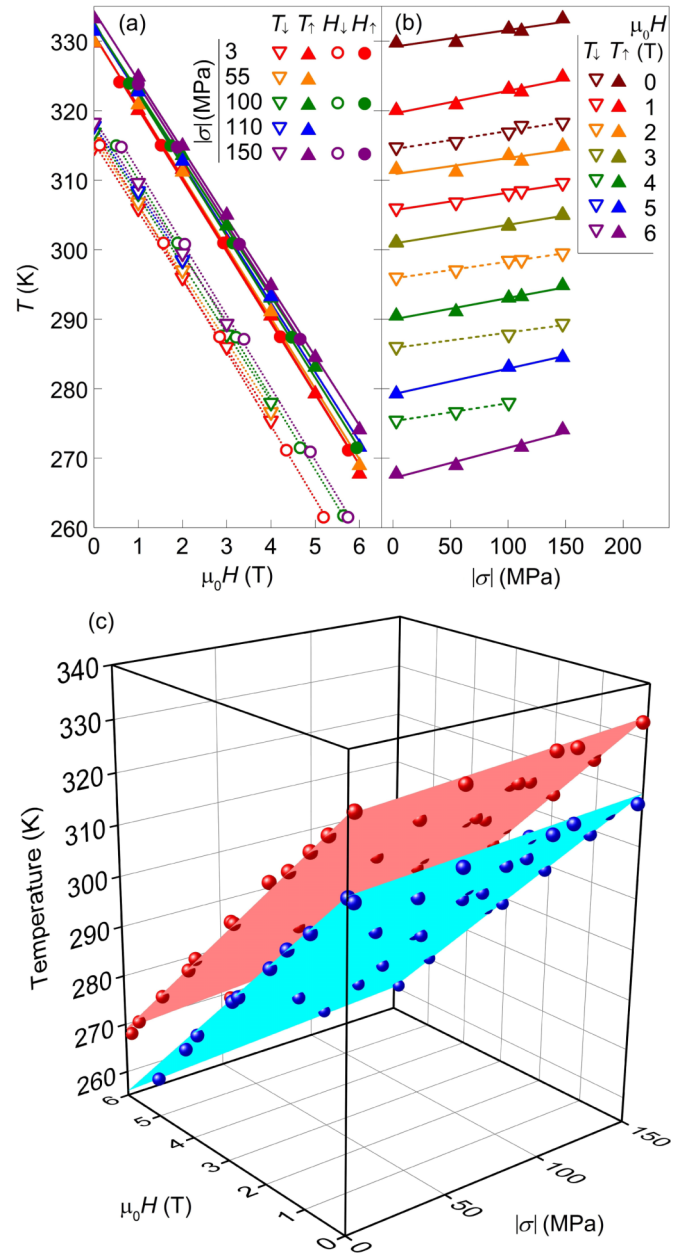

FIG. 3. (a) Transition temperatures as a function of magnetic field (at constant uniaxial compressive stress) and (b) transition temperatures as a function of uniaxial compressive stress (at constant applied magnetic field). Solid symbols correspond to the AFM to FM transiton, and open symbols to the FM to AFM transition. Triangles stand for isofield data and circles, for isothermal data. Lines are linear fits to the experimental data. (c) Transition temperatures as a function of magnetic field and uniaxial compressive stress. Planes correspond to the best fits to the experimental values. Upper red plane corresponds to the AFM to FM transition, and lower blue plane, to the FM to AFM transition.

(exothermal) signals correspond to the FM-AFM transition taking place upon removal of magnetic field. At each value of temperature and uniaxial stress, we identify the transition field as the field value corresponding to the calorimetric peak. Although for isofield measurements [Figs. 2(a) and 2(b)] the poor baseline does not enable a reliable integration of the curves to determine the transition entropy change (ΔS_t), it is possible to identify the transition temperature from the temperature of the calorimetric peak for each value of magnetic field and uniaxial stress. Results are plotted as a function of magnetic field at selected values of uniaxial compressive stress [Fig. 3(a)] and as a function of uniaxial compressive stress at selected values of magnetic field [Fig. 3(b)]. Open triangles correspond to cooling runs (FM-AFM transition) and solid triangles correspond to heating runs (AFM-FM transition). Results from isothermal calorimetric measurements are also included in Fig. 3(a) as circles, where open symbols correspond to the removal of magnetic field (FM to AFM transiton) and solid symbols, to the application of magnetic field (AFM to FM transition).

It is worth noticing that the values found for the transition temperature for each applied magnetic field agree remarkably well regardless of whether temperature or magnetic field is scanned for both AFM-FM and FM-AFM transitions. It is
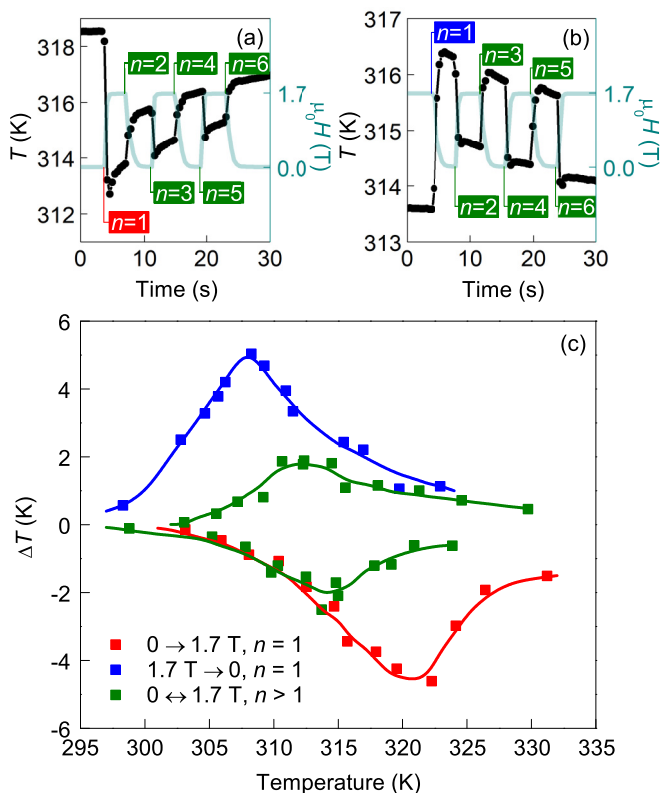
FIG. 4. Illustrative examples of the recorded temperature and magnetic field for heating (a) and cooling (b) protocols under an applied compressive constant stress of 100 MPa. (c) Adiabatic temperature changes corresponding to the application and removal of a 1.7 T magnetic field under a constant compressive stress of 100 MPa. Red and blue symbols correspond to the first ($n = 1$) application and first ($n = 1$) removal of magnetic field for heating and cooling protocols, respectively. Green symbols correspond to the subsequent field cycling ($n > 1$). Lines are guides to the eye.

found that the transition temperature linearly decreases with increasing magnetic field, for all values of applied uniaxial stress. The slope of the T versus H curves does not significantly depend upon the applied stress, with a value $dT/d\mu_0 H = -10.0 \pm 0.4 \, \mathrm{K \, T^{-1}}$, which is in agreement with reported data obtained in the absence of stress [18].

The transition temperature linearly increases with increasing load, indicating a stabilization of the low-volume AFM phase by uniaxial compression. The slope of the T versus $|\sigma|$ does not significantly depend on magnetic field, with a value $dT/d|\sigma| = 0.03 \pm 0.01 \, \mathrm{K \, MPa^{-1}}$.

B. Thermometric measurements

Figures 4(a) and 4(b) illustrate examples of the temperature and magnetic field measurements recorded upon cycling the magnetic field between 0 and 1.7 T. Measurements have been carried out according to the protocols described in Ref. [19], which take into account that application of magnetic field stabilizes the high-temperature FM phase (as heating does) while removal of the field promotes the FM to AFM transition (as cooling does). Consistently with the inverse nature of the magnetocaloric effect in $\mathrm{Fe_{49}Rh_{51}}$, there is a temperature

decrease upon application of magnetic field and a temperature increase when the field is removed. These temperature changes are larger for the first application (removal) of the field and they are reduced (due to hysteresis) and reproducible upon successive field cycling. The measured ΔT values are slightly smaller than previous measurements in the absence of applied stress [19]. This difference is mainly due to the fact that in previous measurements the thermocouple was embedded into the sample, while in present work, it is attached to the sample surface. Furthermore, in present experiments, the sample is in contact (through the PEEK discs) with both the container and the pushing rod which reduces the adiabaticity of the ensemble. The whole set of data measured under a compressive stress of 100 MPa are compiled in Fig. 4(c) for both heating and cooling protocols. Comparison of present data under compressive stress to previous ΔT in the absence of stress [19] shows that the application of uniaxial compressive stress shifts ΔT versus T curves to higher temperatures. We have quantified this shift through the maximum (minimum) of the cooling (heating) curves as $\delta T = 3.1 \pm 0.3 \, \mathrm{K}$, which is consistent with the $dT/d|\sigma| = 0.03 \, \mathrm{K \, MPa^{-1}}$ shift of the AFM-FM transition obtained from calorimetric measurements.

IV. DISCUSSION

A. Phase diagram

Compilation of transition temperatures as a function of magnetic field and uniaxial load provides the complete phase diagram of $\mathrm{Fe_{49}Rh_{51}}$ shown in Fig. 3(c). The great linearity of the transition temperature with respect to the two parameters yields the two planes which separate the FM region (upper part of the diagram) from the AFM region (lower part of the diagram). These planes are $T(H, \sigma) = 329.5 - 10.1\mu_0 H + 0.030|\sigma|$ for the FM to AFM transition and $T(H, \sigma) = 316.1 - 10.0\mu_0 H + 0.026|\sigma|$ for the AFM to FM transition. The region between the two planes is the hysteretic region, and corresponds to a hysteresis in magnetic field $\delta\mu_0 H = 1.3 \, \mathrm{T}$ (independent of stress) and a hysteresis in stress $\delta|\sigma| = 515 \, \mathrm{MPa}$ (independent of magnetic field).

Comparison of present results to earlier data [15] shows that the behavior of Fe-Rh under compressive stress differs from that under tensile stress: transition temperatures increase with increasing compressive stress, while they decrease with increasing tensile stress, thus reflecting a stabilization of the low volume AFM phase by uniaxial compressive stresses and a stabilization of the high-volume FM phase by uniaxial tensile stresses.

Using the reported Young modulus data [27], we have estimated the elastic strain induced by application of 100 MPa stress, which amounts $\sim 0.04 \, \%$ in both FM and AFM phases. This value is about one order of magnitude smaller than the uniaxial strain component of the volume change at the phase transition $\varepsilon \simeq \frac{1}{3}\frac{\Delta v}{v}$, where $\frac{\Delta v}{v}$ is the relative volume change at the FM to AFM phase transition. Since for $\mathrm{Fe_{49}Rh_{51}}$, $\frac{\Delta v}{v} \sim 1\%$ and $\varepsilon \sim 0.33\%$, the relative phase stability between FM and AFM phases with respect to uniaxial stress will be determined by this transition strain and can be accounted for by the

Clausius-Clapeyron equation

$$\frac{dT}{d\sigma} = -\frac{\varepsilon}{\Delta S_t} \simeq -\frac{1}{3}\frac{\Delta v/v}{\Delta S_t}. \qquad (1)$$

For a compressive stress $\sigma < 0$ and $\frac{dT}{d|\sigma|} > 0$, and the low-volume AFM phase is stabilized, while for a tensile stress $\sigma > 0$ and $\frac{dT}{d|\sigma|} < 0$, and the large-volume FM phase is stabilized.

B. Elastocaloric effect

As previously indicated, the poor calorimetric baseline for isofield-isostress temperature scans does not enable a proper integration of thermal curves and no reliable entropy versus temperature curves can be computed. Nevertheless, a good approach to elastocaloric entropy and temperature data can be obtained using a high-quality calorimetric run at zero stress and zero magnetic field, under the assumption that the effect of stress on the $S(T, H, \sigma)$ curves is a pure shift of the curve without any significant change in its shape (see Ref. [6] for details of this method). The reliability of this method in the computation of caloric properties will be discussed in the following section in relation to magnetocaloric data where we compare quasidirect values to data obtained from direct measurements.

In Fig. 5(a), we plot $S(T)$ curves obtained from specific heat data [26] and our differential scanning calorimetry measurements at zero stress and zero magnetic field for heating and cooling runs. The corresponding curves for an applied uniaxial compressive stress of 100 MPa (and zero magnetic field) are also shown. From these curves we have derived elastocaloric adiabatic temperature changes (ΔT) and isothermal entropy changes (ΔS) shown in Figs. 5(b) and 5(c), respectively, for an applied uniaxial compressive stress $|\sigma| = 100$ MPa. A first remarkable result is that the elastocaloric effect is conventional: application of compressive stress adiabatically increases temperature and isothermally reduces entropy. This result is in contrast to an earlier elastocaloric study of Fe-Rh where cooling under the adiabatic application of uniaxial tensile stress was reported [15]. Such a different elastocaloric behavior is in concordance with uniaxial compressive stress promoting the FM to AFM transition and uniaxial tensile stress promoting the AFM to FM transition, as discussed in Sec. IV A. The maximum value for $|\Delta S|$ at 100 MPa is 7.9 J kg^{-1} K^{-1}, lower than the transition entropy change $|\Delta S_t| = 11$ J kg^{-1} K^{-1}, which indicates that a 100 MPa stress is not large enough to induce the transformation of the whole sample. With regards to adiabatic temperature changes, a maximum $|\Delta T| = 2.6$ K is obtained at 100 MPa. This value is close to those measured directly at a larger tensile stress of 150 MPa [15]. It is worth noticing that directly measured ΔT data tend to be lower than estimated values due to the difficulty of performing experiments under fully adiabatic conditions [6].

The elastocaloric $|\Delta S|$ and $|\Delta T|$ values are not expected to be reversible upon stress cycling for the low-stress values studied here. As shown in Fig. 5(a), the shift of the transition induced by application of stress is significantly lower than the thermal hysteresis of the magnetostructural transition. For a low-stress level, the elastocaloric strength quantified as $\frac{|\Delta S|}{|\sigma|} = 0.079$ J kg^{-1} K^{-1} MPa^{-1} and $\frac{|\Delta T|}{|\sigma|} = 0.026$ K MPa^{-1}
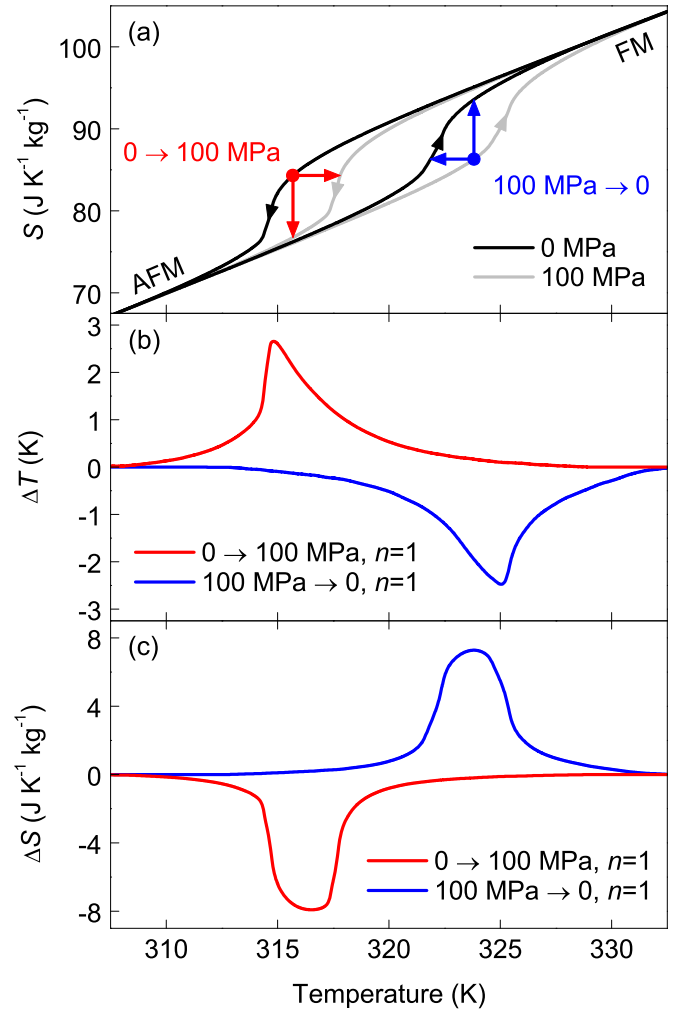

FIG. 5. (a) Entropy as a function of temperature at zero (black curve) and at 100 MPa (grey curve) applied uniaxial compressive stress in the absence of magnetic field. Vertical and horizontal arrows indicate respectively the entropy and temperature changes corresponding to the first ($n = 1$) application and first ($n = 1$) removal of a 100 MPa stress. The resulting adiabatic temperature and isothermal entropy changes are plotted as a function of temperature in (b) and (c). Red color corresponds to the application of stress and blue color to the removal of stress.

is lower than the barocaloric strength, consistently with the lattice distortion at the magnetostructural transition being a pure dilation.

C. Caloric effects under stress and magnetic field

Following a procedure similar to that discussed in the preceding section, we have computed magnetocaloric ΔS and ΔT values in the absence of applied stress and under an applied compressive stress. The excellent agreement between data at zero stress (not shown here) with our earlier studies, obtained from indirect [11], quasidirect [18], and direct [18,19] methods provides a good confidence for the values reported in the present work corresponding to the simultaneous application of magnetic field and uniaxial compressive stress. Here we focus our attention on the effect of uniaxial stress on magnetocaloric
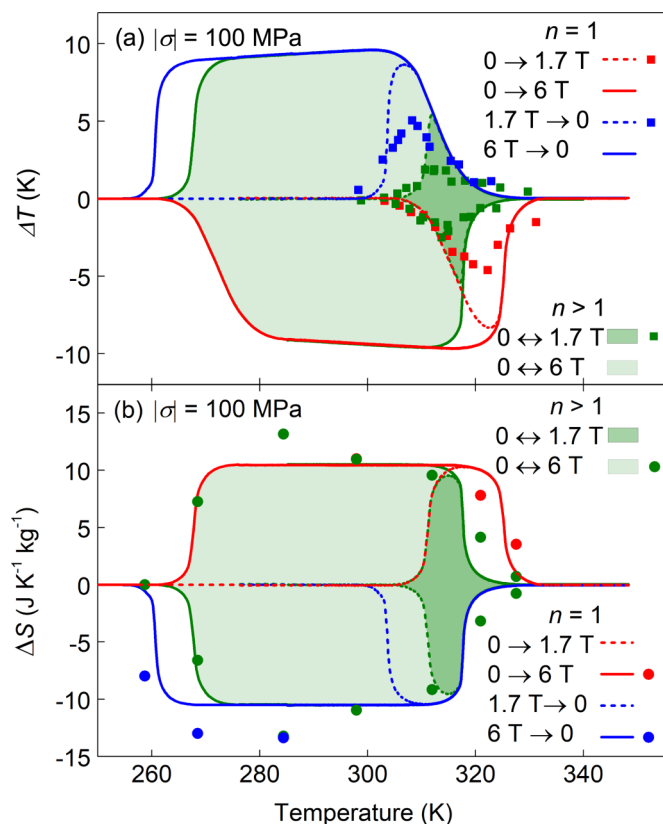
FIG. 6. Adiabatic temperature (a) and entropy (b) changes corresponding to the magnetocaloric effect under an applied uniaxial compressive stress of 100 MPa. Lines correspond to data computed from entropy curves (quasidirect method) where dashed curves correspond to a magnetic field of 1.7 T and solid curves to a magnetic field of 6 T. Symbols stand for directly measured values. Red lines and symbols indicate first ($n = 1$) application of field, blue lines and symbols indicate first ($n = 1$) removal of field, and green lines and symbols indicate successive field cycling. The reversible regions correspond to the green shaded areas.
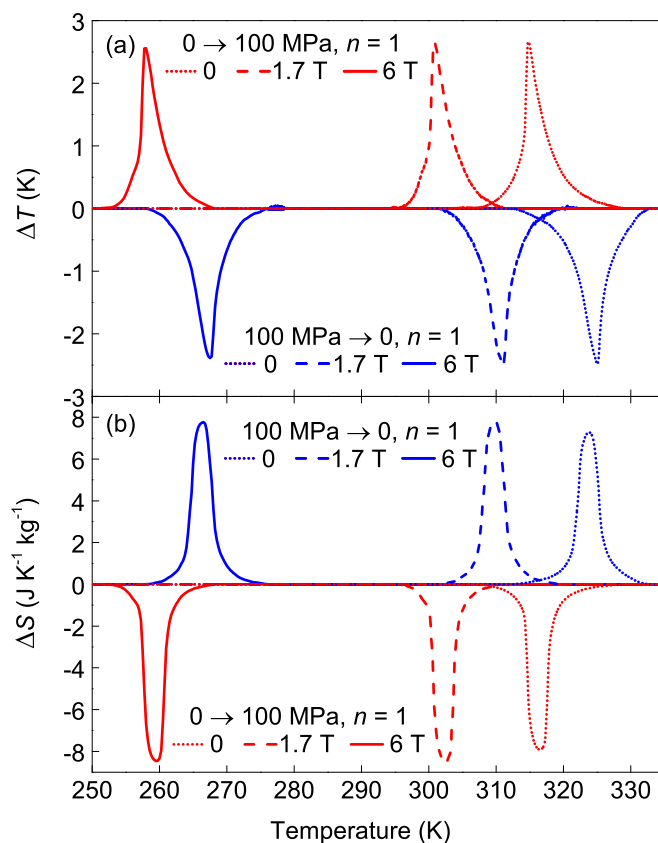

FIG. 7. Adiabatic temperature (a) and entropy (b) changes corresponding to the elastocaloric effect under an applied magnetic field of zero (dotted lines), 1.7 T (dashed lines), and 6 T (solid lines). Red curves correspond to the application of uniaxial compressive stress ($n = 1$) and blue curves to the removal of uniaxial compressive stress ($n = 1$). Data are computed from entropy curves (quasidirect method).

ΔT and ΔS values. Results corresponding to a 100 MPa uniaxial compressive stress are shown as lines in Fig. 6 for magnetic fields of 1.7 and 6 T. Shaded green areas correspond to the reversible regions.

Results from direct measurements of adiabatic temperature changes are shown as solid symbols in Fig. 6(a) for a magnetic field of 1.7 T and an applied uniaxial compression of 100 MPa. Red and blue symbols correspond, respectively, to the first ($n = 1$) application and removal of magnetic field, and green symbols, to values measured under successively ($n > 1$) cycling magnetic field. There is good coincidence between direct and quasidirect ΔT versus T curves but directly measured values are lower than quasidirect ones. This difference is attributed to a nonperfect adiabaticity of thermometric measurements. By comparing measured data to data recorded in the absence of stress [19] (not shown here), it is observed that uniaxial compressive stress shifts ΔT versus T curves to higher temperatures without increasing maximum ΔT values, similarly to what was observed for application of pressure.

Under isothermal conditions, calorimetric thermal curves exhibit a very good baseline [see Figs. 2(c) and 2(d)] and direct

measurements of the isothermal entropy change for application of a field H can be obtained as

$$\Delta S = \frac{1}{T} \int_0^{\mu_0 H} \frac{dQ}{dt} \left(\frac{dH}{dt} \right)^{-1} dH. \qquad (2)$$

For removal of magnetic field, the same expression holds by exchanging integral limits. Results for a magnetic field of 6 T under a constant applied stress of 100 MPa are shown in Fig. 6(b) as solid symbols. Red (blue) symbols correspond to the first application (removal) of magnetic field and green symbols correspond to data for successive cycles. Within experimental uncertainty, there is a good coincidence between direct and quasidirect values. Comparison of ΔS data under applied stress with data in the absence of stress [18] (not shown here) shows that application of stress shifts ΔS versus T curves towards higher temperatures without increasing the maximum ΔS values. This behavior is similar but of lower magnitude to the effect of applying a hydrostatic pressure [11]. The weaker influence of uniaxial stress is consistent with the structural change at the phase transition being a pure dilation.

Finally, it is also worth studying the magnetic field influence on the elastocaloric effect of $Fe_{49}Rh_{51}$. Results for the adiabatic temperature and isothermal entropy changes for an applied

TABLE I. Elastocaloric properties of selected materials. C and I refer to conventional and inverse caloric effects, respectively. For La-Fe-Si, data are predictions based on results discussed in this work.

	Fe$_{49}$Rh$_{51}$	SMA (nonmagnetic)	SMA (magnetic)	La-Fe-Si
Barocaloric, p	C $(dT/dp > 0)$	$(dT/dp \sim 0)$	C $(dT/dp > 0)$	I $(dT/dp < 0)$
Elastocaloric compressive, $\sigma < 0$	C $(dT/d|\sigma| > 0)$	C $(dT/d|\sigma| > 0)$	C $(dT/d|\sigma| > 0)$	I $(dT/d|\sigma| < 0)$
Elastocaloric tensile, $\sigma > 0$	I $(dT/d|\sigma| < 0)$	C $(dT/d|\sigma| > 0)$	C $(dT/d|\sigma| > 0)$	C $(dT/d|\sigma| > 0)$

uniaxial stress of 100 MPa ($n = 1$) are shown in Fig. 7 for applied magnetic fields of 1.7 and 6 T. Application of magnetic field shifts the ΔT versus T and ΔS versus T curves towards lower temperatures without modifying the overall magnitude of the curves. The shift is in concordance with the shift in the transition temperature $dT/d\mu_0 H = 10$ K T^{-1} derived from calorimetric measurements. It is seen that application of moderate fields (<2 T) enables to tune the elastocaloric operation range within a temperature region of ~ 20 K. On the other hand, although for low stresses, the elastocaloric effect is not reversible under stress cycling, a suitable combination of low stresses and low magnetic field provides an enhanced reversibility of the elastocaloric effect. For instance, application of a low magnetic field (<2 T) prior to the removal of compressive stress results in a recovery of the $|\Delta T|$ and $|\Delta S|$ values measured on the loading process in the absence of magnetic field.

D. Comparison to other caloric materials

Given that a thorough comparison of the magnetocaloric properties of Fe$_{49}$Rh$_{51}$ to those of other giant magnetocaloric materials was previously reported [21], in this section, we focus on the elastocaloric properties. Prototype elastocaloric materials are shape memory alloys. These alloys undergo a martensitic transition, which can be driven by uniaxial stress, and the latent heat of this transition provides the major contribution to the elastocaloric entropy change [6]. Shape memory alloys include both magnetic and nonmagnetic materials, where the former also exhibit giant magnetocaloric [28] and barocaloric [8] effects. There are a number of noticeable differences between the elastocaloric effect in Fe$_{49}$Rh$_{51}$ and that in shape memory alloys. First, the sensitivity of the transition temperature to applied stress is significantly lower $(dT/d|\sigma| \sim 0.03$ K MPa$^{-1})$ in Fe$_{49}$Rh$_{51}$ than in martensitic materials (typically in the range $dT/d|\sigma| \sim 0.1$–1 K MPa^{-1}). Such a weaker sensitivity is a consequence of the lower uniaxial strain during the transition ($\varepsilon \sim 0.33\%$ in Fe$_{49}$Rh$_{51}$ and $\varepsilon \sim 3\%$–10% in shape memory alloys) [6].

Interestingly, in Fe$_{49}$Rh$_{51}$, the transition temperature increases with increasing compressive stress while it decreases with increasing tensile stress. This is in contrast to the behavior found for shape memory alloys for which the transition temperature increases for both increasing compressive and tensile stresses. Such a different behavior is due to the intrinsic nature of the structural transition in the two alloy systems. In shape memory alloys, the low-temperature phase (martensite) results from a shear mechanism. Symmetry enables a number of deformation modes, and the material selects the mode associated with the development of a ferroelastic domain (martensitic variant) that has the most favorable orientation to the applied

stress. According to this mechanism, $\varepsilon < 0$ for compressive uniaxial stress, while $\varepsilon > 0$ for tensile uniaxial stress [29]. On the other hand, in Fe$_{49}$Rh$_{51}$, the transition from the high-(FM) to the low- (AFM) temperature phase involves a pure dilation ($\Delta v < 0$), which results in $\varepsilon < 0$ for both compressive and tensile uniaxial stresses. The differences in the relative phase stability with respect to compressive and tensile stresses give rise to a different elastocaloric behavior: while for shape memory alloys the elastocaloric effect is conventional for both compressive and tensile stresses, the elastocaloric effect in Fe$_{49}$Rh$_{51}$ is conventional for compressive stresses and inverse for tensile stresses.

The measured isothermal entropy ($|\Delta S| = 7.9$ J kg^{-1}K^{-1}) and adiabatic temperature ($|\Delta T| = 2.6$ K) changes for the elastocaloric effect in Fe$_{49}$Rh$_{51}$ under 100 MPa are lower than typical values for shape memory alloys at similar stress values ($|\Delta S| \sim 10$–20 J kg^{-1} K^{-1}, $|\Delta T| = 5$–10 K) [6]. These lower values are basically due to a lower transition entropy change and also to a weaker sensitivity of the transition temperature to stress.

The similarities and differences in the elastocaloric properties of different alloy families compiled in Table I provide a guide to anticipate the unexplored elastocaloric behavior of other giant caloric materials. As an example we discuss La-Fe-Si, which undergoes a magnetostructural transition with associated giant magnetocaloric [30] and barocaloric effects [31]. Upon cooling, this material transforms from a high-temperature paramagnetic phase to a low-temperature ferromagnetic phase, with a pure dilation ($\frac{\Delta v}{v} \sim 1\%$) of the cubic unit cell ($Fm\bar{3}c$ space group). The larger volume of the low-temperature FM phase gives rise to an inverse barocaloric effect, and it can be anticipated that the transition temperature will shift to lower values for compressive stresses and to higher values for tensile stresses. This behavior will give rise to a conventional elastocaloric effect for tensile stresses and inverse elastocaloric effect for compressive stresses.

Therefore the mechanocaloric performance of a given material can always be optimized by choosing the mechanical field that best tailors the symmetries of the phase transition. In some cases, this also involves tunability of the temperature window at which the caloric effect is exhibited by switching its conventional character to inverse, or vice versa.

V. SUMMARY AND CONCLUSIONS

We have used bespoke experimental systems to study the giant caloric response of Fe$_{49}$Rh$_{51}$ subjected to uniaxial compressive stresses and magnetic field. We have shown that the behavior of Fe$_{49}$Rh$_{51}$ under compressive stress differs from that under tensile stress: compressive stresses stabilize the AFM phase (increase in the magnetostructural transition

temperature) while tensile stresses stabilize the FM phase (decrease in the magnetostructural transition temperature). In concordance with this behavior, $Fe_{49}Rh_{51}$ exhibits the conventional elastocaloric effect for compressive stresses and the inverse elastocaloric effect for tensile stresses.

We have also studied the caloric response of $Fe_{49}Rh_{51}$ arising from the combined action of magnetic field and compressive uniaxial stresses. No significant increase in the maximum values for adiabatic temperature and isothermal entropy changes corresponding to the elastocaloric and magnetocaloric effects has been found when a secondary (nonconjugated) field was applied. The transition hysteresis in temperature, magnetic field, and uniaxial compressive stress has been found to be constant, independent of the application of a secondary field.

Application of a secondary field shifts the temperature window where giant elastocaloric and magnetocaloric effects occur. This sensitivity to a secondary field enables tuning of hysteresis by the combined action of two fields and opens up the possibility of designing devices that take advantage of this property. In particular, an enhancement of the reversibility of a specific caloric effect can be achieved by a suitable choice of magnetic field and uniaxial stress. It is also worth mentioning that the possibility of exploiting hysteresis for efficient cooling has been recently been put forward [32], and the behavior found here for $Fe_{49}Rh_{51}$ under magnetic field and uniaxial stress makes this material an excellent candidate for this newly proposed cooling strategy.

[1] S. Fähler *et al.*, Adv. Eng. Mater. **14**, 10 (2012).

[2] L. Mañosa, A. Planes, and M. Acet, J. Mater. Chem. A **1**, 4925 (2013).

[3] X. Moya, S. Kar-Narayan, and N. D. Mathur, Nat. Mater. **13**, 439 (2014).

[4] K. A. Gschneidnder, V. K. Pecharsky, and A. O. Tsokol, Rep. Prog. Phys. **68**, 1479 (2005).

[5] M. Valant, Prog. Mater. Sci. **57**, 980 (2012).

[6] L. Mañosa and A. Planes, Adv. Mater. **29**, 1603607 (2017).

[7] E. Bonnot, R. Romero, L. Mañosa, E. Vives, and A. Planes, Phys. Rev. Lett. **100**, 125901 (2008).

[8] L. Mañosa *et al.*, Nat. Mater. **9**, 478 (2010).

[9] J. Liu, T. Gotshcall, K. P. Skokov, J. D. Moore, and O. Gutfleisch, Nat. Mater. **11**, 620 (2012).

[10] E. Mendive-Tapia and T. Castán, Phys. Rev. B **91**, 224421 (2015).

[11] E. Stern-Taulats *et al.*, Phys. Rev,. B **95**, 104424 (2017).

[12] E. Stern-Taulats, T. Castán, L. Mañosa, A. Planes, N. D. Mathur, and X. Moya, MRS Bull. **43**, 295 (2018).

[13] L. Mañosa and A. Planes, J. Phys D: Appl. Phys. **51**, 070201 (2018) and references therein.

[14] S. Nikitin, G. Myalikgulyev, A. M. Tishin, M. P. Annaorazov, K. A. Asatryan, and A. L. Tyurin, Phys. Lett. A **148**, 363 (1990).

[15] S. Nikitin, G. Myalikgulyev, M. P. Annaorazov, A. L. Tyurin, R. W. Myndev, and S. A. Akopyan, Phys. Lett. A **171**, 234 (1992).

[16] V. K. Pecharsky and K. A. Gschneidner, Phys. Rev. Lett. **78**, 4494 (1997).

[17] L. H. Lewis, C. H. Marrow, and S. Langridge, J. Phys. D: Appl. Phys. **49**, 323002 (2016).

[18] E. Stern-Taulats, A. Planes, P. Lloveras, M. Barrio, J.L. Tamarit, S. Pramanick, S. Majumdar, C. Frontera, and L. Manosa, Phys. Rev. B, **89**, 214105 (2014).

[19] E. Stern-Taulats *et al.*, App. Phys. Lett. **107**, 152409 (2015).

[20] A. Chirkova, K. O. Skokov, L. Schultz, N. V. Baranov, O. Gutfleisch, and T. Woodcok, Acta Mater. **106**, 15 (2016).

[21] K. Sandeman, Scripta Mater. **67**, 566 (2012).

[22] G. Shirane, R. Nathans, and C. W. Chen, Phys. Rev. **134**, A1547 (1964).

[23] N. A. Zarkevich and D. D. Johnson, arXiv:1702.03042v4.

[24] A. Gràcia-Condal, E. Stern-Taulats, A. Planes, E. Vives, and L. Mañosa, Phys. Status Solidi B, **255**, 1700422 (2018).

[25] Given that $\sigma < 0$ for compressive stresses, we will analyze our data in terms of the magnitude of the applied compressive stress $|\sigma|$.

[26] D. W. Cooke, F. Hellman, C. Baldasseroni, C. Bordel, S. Moyerman, and E. E. Fullerton, Phys. Rev. Lett. **109**, 255901 (2012).

[27] U. Aschauer, R. Braddell, S. A. Brechbül, P. M. Derlet, and N. A. Spalding, Phys. Rev. B **94**, 014109 (2016).

[28] A. Planes, L. Mañosa, and M. Acet, J. Phys. Condens. Matter. **21**, 233201 (2009).

[29] V. Novak and P. Sittner, Mat. Sci. Eng. A **378**, 490 (2004).

[30] A. Fujita, S. Fujieda, Y. Hasegawa, and K. Fukamichi, Phys. Rev. B **67**, 104416 (2003).

[31] L. Mañosa, D. Gonzàlez-Alonso, A. Planes, M. Barrio, J. L. Tamarit, I. S. Titov, M. Acet, A. Bhattacharyya, and S. Majumdar, Nat. Commun. **2**, 595 (2011).

[32] T. Gotschall *et al.*, Nat. Mater. (to be published).